AUBURN UNIVERSITY
ENGINEERING EXPERIMENT STATION

FRACTURE ANALYSIS OF RADIAL SCIENTIFIC INSTRUMENT MODULE REGISTRATION FITTINGS OF THE SPACE TELESCOPE

Interim Report: January 15, 1985 - August 30, 1985
Contract Number: NAS8—36287

Submitted by: Auburn University
Engineering Experiment Station
Auburn University, Alabama 36849

Prepared by: C.W. Springfield, Jr.
Department of Civil Engineering
Auburn University
Auburn University, Alabama 36849

Prepared for: George C. Marshall Space Flight Center
Marshall Space Flight Center, Alabama 35812

September 3, 1985

FRACTURE ANALYSIS OF RADIAL SCIENTIFIC INSTRUMENT MODULE REGISTRATION FITTINGS OF THE SPACE TELESCOPE

INTERIM REPORT: January 15,1985 - August 30,1985
Contract Number: NAS8-36287
Submitted by: Auburn University
Engineering Experiment Station
Auburn University, Alabama 36849

Prepared by: C.W. Springfield, Jr.
Department of Civil Engineering
Auburn University
Auburn University, Alabama 36849

Prepared for: George C. Marshall Space Flight Center
Marshall Space Flight Center, Alabama 35812

September 3, 1985

TABLE OF CONTENTS

INTRODUCTION

The space telescope contains various scientific instrument (SI) modules which are mounted to the Focal Plane Structure (FPS) in a statically determinate manner. This is accomplished by using three registration fittings per SI module, one resisting three translations, another resisting two and the third resisting only one. Due to thermal insulating requirements these fittings are complex devices composed of numerous pieces. The structural integrity of these fittings is of great importance to the safety of the orbiter transporting the telescope, so in addition to the stress analyses performed during the design of these components, fracture susceptibility also needs to be considered. In this work the pieces of the registration fittings for the Radial SI Module containing the Wide Field Planetary Camera were examined to determine which would endanger the orbiter if they fractured and what is the likelihood of their fracture. The latter is stated in terms of maximum allowable initial flaw sizes in these pieces.

When possible, pieces of the fittings where shown to be fail-safe through redundancy. Primarily this was done for the bolts in four bolt connections. For these it was shown that the loss of one bolt would not destroy the connection. For pieces in nonredundant configurations fatigue fracture analyses were performed.

In order to determine the maximum allowable initial flaw sizes, fatigue fracture analyses were performed using the

FLAGRO4 computer program written by T. Hu of Rockwell International [1]. This program integrates the crack growth rate per cycle equation of Collipriest [2] for a given geometry and load spectrum, beginning at a specified initial flaw size and ending when fracture instability occurs. Given the desired length of service of the parts, this program was used iteratively to determine the maximum allowable initial flaw sizes. In this work the desired length of service was taken to be four lifetimes, with a lifetime being defined as one application of the load spectrum given in Table 2.

Some of the pieces are bolts or other threaded rods. If a flaw exists at the root of a thread then there is some interaction of the two stress raising effects; i.e., the stress concentration due to the thread and the stress singularity (if Linear Elastic Fracture Mechanics methods are used) due to the flaw. The extent of this interaction is not yet well defined. In order to obtain conservative estimates of allowable initial flaw size for these pieces, a fracture analysis code called ROD, developed by C. Meyers of MSFC, which also uses the Collipriest crack growth rate equation and includes the capability of analyzing a rod with an external circumferential crack, was used by treating the thread depth as part of the flaw size. These estimates are included in this report. However, inasmuch as the possible fracture of threaded parts is a common issue in structural analysis it was decided to investigate the stress concentration/stress singularity interaction to determine appropriate methods of stress

FLAGRO4 computer program written by T. Hu of Rockwell International [1]. This program integrates the crack growth rate per cycle equation of Collipriest [2] for a given geometry and load spectrum, beginning at a specified initial flaw size and ending when fracture instability occurs. Given the desired length of service of the parts, this program was used iteratively to determine the maximum allowable initial flaw sizes. In this work the desired length of service was taken to be four lifetimes, with a lifetime being defined as one application of the load spectrum given in Table 2.

Some of the pieces are bolts or other threaded rods. If a flaw exists at the root of a thread then there is some interaction of the two stress raising effects; i.e., the stress concentration due to the thread and the stress singularity (if Linear Elastic Fracture Mechanics methods are used) due to the flaw. The extent of this interaction is not yet well defined. In order to obtain conservative estimates of allowable initial flaw size for these pieces, a fracture analysis code called ROD, developed by C. Meyers of MSFC, which also uses the Collipriest crack growth rate equation and includes the capability of analyzing a rod with an external circumferential crack, was used by treating the thread depth as part of the flaw size. These estimates are included in this report. However, inasmuch as the possible fracture of threaded parts is a common issue in structural analysis it was decided to investigate the stress concentration/stress singularity interaction to determine appropriate methods of stress

intensity factor calculation for these geometries, and, thus, to be able to make more accurate crack growth predictions, not only for the threaded pieces of the registration fittings being analyzed here, but also for future fracture analyses of such parts. The results of this investigation will be included in the final report.

This project was divided into four Tasks. In Task I the identification of required fracture analyses was accomplished. In Task II the FLAGRO4 code, furnished by MSFC, was implemented on Auburn University's IBM 3033 computer. In Task III stress analyses needed in addition to those used in the original design of the fittings were performed. These were needed to supply suitable input data for the fracture analyses which were performed as Task IV. This report, however, is not divided by Tasks but, instead, by fittings, these being identified by their location at points A, B or C, as indicated in Figure 1. Also shown in Figure 1 are the global coordinate directions, V_1, V_2 and V_3, for the structure. Forces applied in these directions are identified as A_1, A_2, A_3 at point A, B_1 at point B, etc. Table 1 shows the loads in these directions for the various events in the service of the telescope, and Table 2 shows the loading spectrum used in the fatigue fracture analyses of parts which experience complete load reversals. Some parts are loaded only during the positive or negative half of the load cycles. Some are subjected to a pretension. For these the spectrum in Table 2 was modified appropriately. The methods of analysis used and results obtained for each piece of

each fitting are reported.

REGISTRATION FITTING AT POINT A

The various pieces of the registration fitting at point A which were addressed in this work are listed in Table 3. Also shown are the materials of which each is made, the threshold stress intensity factor range, ΔK_o, of each, and the fracture toughness, K_c, of each, as well as the manner in which their fracture susceptibility was treated; i.e., a piece is listed as fail-safe or else its maximum allowable initial flaw size is specified. These are discussed as the remainder of this section.

Focal Plane Structure Side

The base (679-3973) which mounts to the FPS is shown in Figure 2. The most likely fracture scenario identified for the base was the growth of a through crack located as indicated in the figure. The loading on this crack was assumed to be due to loads applied in the V_2 direction, resisted equally by the two shear lugs. Thus, half of the load was used as a tensile stress on a central through crack model as given in Figure 3, with w = 3.0 inches, t = 0.718 inches and $\sigma_g = 0.3646 \times A_2$ ksi. This stress, σ_g, is either the stress σ_A, σ_{LO} or σ_L of Table 2 if A_2 is due to Acoustic, Lift-Off or Landing loads, respectively. From Table 1 it is found that the largest value of A_2 is 0.77 kips which is due to Lift-Off. Steps 8 and 16 of

the spectrum in Table 2 give the largest stress range, then, it being 0.56 ksi. With this applied loading a crack length equal to the plate width would not be large enough to reach the threshold stress intensity factor range of 7 ksi-inch$^{0.5}$ for this titanium alloy. It was concluded, then, that fracture would not occur in the base.

Three flexures (679-4132) are designed to transmit force A_3 from the ball retainer to the cover. This causes the bending stress in the flexures. However, loads A_1 and A_2, which are primarily resisted by the three radial shear slugs, cause axial forces in these flexures since the applied loads, the shear slugs and the flexures are not coplanar. This is illustrated in Figure 4, and the locations of the flexures in their V_1-V_2 plane is also shown. For fracture the largest tensile stresses are the ones of interest, and this occurs in the flexure identified as F_8 in Figure 4. It was modeled as a cantilever beam with its movable end restrained against rotation, this end being loaded transversely and axially by concentrated forces. This is shown in Figure 5. The bending stress is σ_b = 19.07 x A_3 ksi, and the tensile stress due to axial loading is σ_t = 9.53 x A_1 ksi. For this particular flexure the A_2 loading did not contribute to the stress. A fatigue fracture analysis was performed on the model shown in Figure 5 considering an edge crack subjected to both tension and bending using FLAGRO4. In the load spectrum of Table 2, the stresses, σ_A, σ_{Lo} and σ_L, are the sum of the bending and tensile stresses. The FLAGRO4 program then uses the correct

proportions of these in tension and bending. The maximum allowable initial flaw size for four lifetimes was found to be, a_o = 0.022 inches.

The loads acting on the flexures are transferred to the aluminum cover (679-4135). They subject the cover alternately to tension and bending and then to compression and reversed bending, as is shown in Figure 6. The bending moment is due to the lateral force, F, and the force reacting it which is provided by the internal spacer. Their lines of action are assumed to be separated by a distance, e = 0.903 inches. The axial loading results from A_3. Neither of the fatigue fracture computer programs being used has the capability to treat a cylinder subjected to both tension and bending, so a fracture model as is shown in Figure 3 was used in FLAGRO4 to represent half of the cylinder, albeit flattened into a plate. In this model w = 2.75 inches, which is half of the cover circumference, t = 0.25 inches, the cover wall thickness at the point of interest, and $\sigma_g = 1.68 \times F + 0.728 \times A_3$ ksi, with $F = 0.857 \times (A_1^2 + A_2^2)^{0.5}$ kips. It was found that for a crack half-length of over 1.3 inches no crack propagation will occur.

A bolt (679-5280) holds the aluminum cover in place. The bolt has a pretension of 8.24 kips. When A_1, A_2, A_3 are positive this bolt is subjected to an additional tension of $A_3 + 1.2 \times F$ kips, with F defined as in the preceding paragraph. When the negatives of these are applied, the bolt does not carry the A_3 load, but there is still a tensile contribution due to the 1.2 x F load. As a result every cycle of loading produces two

cycles of tension in the bolt. In order to simplify the analysis in a conservative manner, it was assumed that the A_3 loading produces tensile stress in the bolt on its negative cycle also so that every cycle would experience the same maximum stress. The cross sectional area of the bolt is 0.1504 square inches, yielding a minimum stress in the bolt of 54.8 ksi and a maximum stress of 54.8 + σ_g ksi, with $\sigma_g = (A_3 + 1.2 \times F)/0.1504$ ksi, for each cycle of loading. Thus, the terms in the Maximum column of Table 2 must have the 54.8 ksi prestress added to them, all the terms in the Minimum column are simply this prestress, and in the Cycles column each number is multiplied by two. Using this load spectrum in the ROD program it was determined that fracture instability would be reached at four lifetimes for an initial circumferential flaw size of 0.069 inches. However, net section yielding will occur in this piece before fracture instability, so analyses were performed to determine what initial flaw size would produce net section yielding at four lifetimes. This flaw size was found to be 0.035 inches.

The bolt which holds the aluminum cover in place mates with an internally threaded portion of the ball lower retainer (679-4130-111). This is illustrated in Figure 7. The threaded portion experiences the same load spectrum as the bolt except that the tensile area of this piece is different. In this analysis the minimum stress was 40.6 ksi and the maximum stress was given by 40.6 +$(A_3 + 1.2 \times F)/0.2029$ ksi. The ROD program used in the analysis of the bolt does not treat internally

threaded pieces, so the threaded portion of the lower retainer was treated as a plate of width, w = 1.61 inches, which is the circumference at its average diameter. Its plate thickness, t = 0.126 inches, is the difference between the outer radius of the piece (0.312 inches) and the root radius of a 7/16 inch bolt (0.186 inches). Instead of a central through crack, a through edge crack was considered, the depth of this crack being the thread depth plus an initial flaw depth, and the applied stress was assumed to be uniform. In this way it is felt that an approximation to an internal circumferential flaw was achieved. The results of this analysis predict an allowable initial flaw size of 0.011 inches.

The ball upper retainer is attached to the lower retainer by four bolts (NAS 1351) which were checked for redundancy. Figure 7 shows the retainer and the location of these bolts. In order to demonstrate the redundancy of these bolts it was assumed that one of the bolts was missing and that the other three would carry the tension and compression required to hold the fitting. The missing bolt was assumed to be the one in the fourth quadrant of the V_1-V_2 plane, and the Lift-Off values of A_1, A_2, A_3 were used to compute the maximum tensile stress in a remaining bolt. A pretension of 2.9 kips was also applied. The maximum tensile stress in a bolt thus calculated was found to be 76.4 ksi which is less than the ultimate tensile strength of the bolt, S_{ut} = 80 ksi. Consequently, it was determined that three bolts are capable of carrying the load, making this connection fail-safe, and that no fracture analysis is

necessary for these.

Four bolts (NAS 1005) are used to attach the base to the FPS. These were checked for redundancy in the same manner as the ball retainer connecting bolts. The location of these bolts is shown in Figure 2. Loads A_1 and A_2 were taken to be acting in a plane located 1.25 inches above the base/FPS interface for moment calculations. The bolt assumed to be missing is the one located in the third quadrant of the V_1-V_2 plane. Again using the Lift-Off values of the applied loads and a pretension of 3.09 kips the maximum tensile stress in a bolt was found to be 102 ksi which is less than the ultimate tensile strength of 140 ksi. Thus, this connection is fail-safe, and a fracture analysis of these bolts is not required.

Scientific Instrument Side

The base on the SI side of the point A fitting (679-2152) is shown in Figure 8. A possible fracture because of a through crack located as shown in the figure was investigated. The procedure and results are quite similar to those used and discovered for the base on the FPS side; that is, the loading was half of A_2 applied to a fracture model as shown in Figure 3, but with w = 3.24 inches, t = 0.88 inches and σ_g = 0.263 x A_2 ksi. As with the other base this stress is too small to develop a stress intensity factor range as large as the threshold value for any possible crack size.

For the jackhead (679-2230) the critical location for a

flaw is in the thread relief grove, as indicated in Figure 9. This was analyzed using the ROD program assuming a circumferential crack with a depth equal to the groove depth plus an initial crack depth. Loads A_1 and A_2 cause the same tensile stress in the jackhead during both the positive and negative halves of the loading cycles, while the A_3 load causes tensile stress during the positive half of the cycle and no stress during the negative half. As was done in the analysis of the bolt which fastens the aluminum cover, it was assumed that the tension due to A_3 loading occurs in both halves of the loading cycle so that the number of cycles in the load spectrum of Table 2 may simply be multiplied by two. This results in a crack growth rate somewhat larger than actually exists, so a conservative analysis is obtained. The cross sectional area of the jackhead is 0.1963 square inches, and a pretension of 4.84 kips is applied, so the Minimum stresses in the loading spectrum are always 24.7 ksi. The Maximum stresses in the spectrum are given by $24.7 + (A_3 + F)/0.1963$ ksi, in which $F = 0.813 \times (A_1^2 + A_2^2)^{0.5}$. The fatigue fracture analysis predicted a maximum allowable initial flaw depth of 0.084 inches to reach fracture instability at four lifetimes, but as is the case with the aluminum cover attachment bolt, net section yielding will occur prior to fracture instability. In order to reach net section yielding not before four lifetimes an initial flaw depth of 0.032 inches is maximum.

The bolts (NAS 1005) which attach the base to the SI were checked for redundancy in the manner used for the bolts

fastening the base on the FPS side of the fitting. Figure 8 shows the locations of these bolts, and the one in the third quadrant of the V_1-V_2 plane was assumed to be missing. Lift-Off loads were used along with a pretension of 3.07 kips. The A_1 and A_2 loads were assumed to act in a plane 1.87 inches above the base/SI interface. A maximum tensile stress in a remaining bolt was determined to be 116 ksi which is less than the ultimate strength, S_{ut} = 140 ksi, so this connection is also fail-safe.

REGISTRATION FITTING AT POINT B

Table 4 lists the various pieces of the registration fitting at point B which were considered in this work. The format of this table is like that of Table 3 for the fitting at point A. Except for the support plate on the SI side of the fitting, the pieces of this fitting are identical to those of the fitting at point C. Inasmuch as the loads are greater at point C, the results obtained from analyses at point C are taken as conservative results at point B. To see the details of the analyses for all the pieces of the point B fitting except the support plate the reader is referred to the section of this report titled "REGISTRATION FITTING AT POINT C". The geometry and loading of the point B support plate (679-2228) are sufficiently different from the support plate at point C that they were analyzed independently.

In order to identify likely fracture locations and to

determine the states of stress at these locations in the support plate at point B, a plane stress analysis of the support plate was performed using the SAP V finite element program [3]. The finite element model used is shown in Figure 10, along with the locations at which flaws were assumed to exist. The cut-out region in which the flexure fits was modeled by reducing the Young's modulus of the elements in that region by the ratio of the reduced thickness to the thickness of the rest of the piece. As can be seen in Figure 10, only a portion of the support plate was modeled, the remainder being treated as rigid. The most critical location found for a crack in this piece is indicated in the figure. The stress distribution at this location can be represented by that due to a combination of bending and axial loading, these being found to be given by $\sigma_b = 2.9 \times B_1$ ksi and $\sigma_t = 2.5 \times B_1$ ksi. These only occur during half of a load cycle, so the stresses in the Minimum column of Table 2 were taken to be zero. An analysis of an edge crack was performed, and it was determined that an initial crack depth of 0.153 inches is acceptable.

REGISTRATION FITTING AT POINT C

Following the format of Tables 3 and 4, Table 5 lists the pieces of the point C registration fitting which were addressed in this project along with the material, fracture toughnesses, and fracture susceptibility of each. A description of the various analyses is given in the following paragraphs.

Focal Plane Structure Side

Two possible flaw locations were investigated in the base (911-4236), these being illustrated in Figure 11 which shows two views of the base with the ball installed. At location 12 is a through crack subjected to stresses due to the C_1 loads. The fracture model is as shown in Figure 3 with w = 4.50 inches, t = 0.5 inches and σ_g = 0.349 x C_1 ksi. As was found to be the case with the other bases, even when C_1 is due to Lift-Off this applied stress is not large enough to cause crack growth for any flaw size which can occur. The other flaw which was considered was an edge crack at location 12a. At this location the C_2 load causes both a uniform tension load and a bending load. The resulting stress is found to be σ_g = 1.44 x C_2 ksi on the ball side of the piece, and it was assumed to decay linearly to zero on the back side. In the load spectrum of Table 2, σ_g is either σ_A, σ_{LO} or σ_L, when the applied loads are due to either Acoustic, Lift-Off or Landing sources, respectively. These stresses were divided into the appropriate tensile and bending stresses in the FLAGRO4 program in the analysis. It was found that an edge crack depth in excess of 1.5 inches would be required to develop net section yielding which will occur before fracture instability.

The stress relief groove on the stem of the ball (679-2387-110) is the most critical potential flaw location in this piece. A circumferential flaw was assumed to exist there, as is shown in Figure 12. The cyclic loading is tension due to

the force, $F = (C_1^2 + C_2^2)^{0.5}$, during both the positive and negative halves of the loading cycles. Thus the numbers in the Cycles column of Table 2 were doubled, those in the Minimum column were the prestress of 14.4 ksi and those in the Maximum column were 14.4 + F/0.3068 ksi. It was determined that net section yielding would occur before fracture instability, at which time the flaw would have become 0.1485 inches deep. This depth is predicted to be reached at four lifetimes by a flaw of initial depth, a_o = 0.1475 inches.

Four bolts (NAS 1005) fasten the base to the FPS. They were checked for redundancy in a manner similar to those of the other bases. The bolt locations are shown in Figure 11, and it was assumed that the C_1 load acts in a plane 3.14 inches above the base/FPS interface. The worst condition arises when the bolt in the fourth quadrant of the V_3-V_1 plane is missing. Assuming this bolt to be missing and a pretension of 3.09 kips, the highest remaining bolt tension was determined to be 5.88 kips, or 101 ksi. This is smaller than the ultimate tensile strength of the bolt, S_{ut} = 140 ksi, so this connection is fail-safe.

Scientific Instrument Side

The ball on the FPS side fits into the support plate (679-2223). As was done for the support plate in the point B fitting, a plane stress analysis was performed using the SAP V finite element program. The model used is shown in Figure 13. As is clear from the figure only a portion of the support plate

was modeled, the remainder being assumed to be rigid. The regions which are cut-out to accept the flexures were modeled by reducing the Young's modulus of the elements in these regions by the percentage that the material is actually reduced. Also shown in Figure 13 is the most critical location for the existence of an edge crack. At this cross section the stress can be represented by a contribution due to uniform axial stress and a contribution due to pure bending, σ_t = 1.75 x C_1 + 0.85 x C_2 ksi and σ_b = 2.71 x C_1 + 0.73 x C_2 ksi, respectively. Because these only occur during half of a load cycle, the minimum stresses in the applied load spectrum were taken to be zero. Net section yielding, defined in this particular analysis as the development of a plastic hinge at this cross section, is the limiting condition here. So the maximum allowable initial flaw depth for an edge crack at this location is the depth which will grow such that the cross section is reduced to a size allowing net section yielding at four lifetimes. This initial flaw depth was found to be 0.21 inches.

The support plate is connected to the base (679-2211) by three bolts. The base attaches to the SI with four bolts. This is shown in Figure 14. The possible fracture due to though cracks emanating from a bolt hole as shown in the figure was considered. Loading at this bolt was assumed to be one-third of the applied C_1. A fracture model as is shown in Figure 15 was analyzed with w = 2.125 inches, t = 0.58 inches and the applied stress, σ_g = 0.2705 x C_1. It was determined

that the threshold stress intensity factor range would not be reached for any possible initial crack size.

Since three bolts (NAS 1005) connect the support plate to the base rather than four, this connection was not checked for redundancy, but instead a fracture analysis was performed on the bolt subjected to the highest loading. This bolt is indicated in Figure 14. In addition to the preload of 3.07 kips, it is subjected to a fluctuating load of 0.434 x C_1 kips during half of a loading cycle and zero during the other half. In view of this, the minimum stresses were taken to be the prestress and the maximum stresses were the sum of the prestress and the fluctuating stress. A circumferential flaw which is 0.027 inches deep will cause net section yielding, but this flaw does not grow when subjected to the stress intensity factor range corresponding to the applied fluctuating stresses. Therefore, the maximum allowable initial circumferential flaw depth is 0.027 inches.

The four bolts (NAS 1005) which were used to attach the base to the SI were checked for redundancy. Their locations are indicated in Figure 14. The C_1 load was assumed to act in a plane 2.45 inches above the base/SI interface, and the bolt in the first quadrant of the V_3-V_1 plane was the one assumed to be missing. The largest bolt tension due to the applied loads, which were the Lift-Off loads, was found to be 2.1 kips. This load along with the preload of 3.09 kips causes a tensile stress in the bolt of 89.5 ksi. The ultimate tensile strength of the bolt is 140 ksi, so this connection is deemed fail-safe.

REMARKS

Various pieces of the registration fittings for the Radial SI module of the Space Telescope have been examined from a fracture mechanics point of view and deemed to be fail-safe or else have had maximum allowable flaw sizes specified for them. The results of these analyses are summarized in Tables 3 - 5 and also in the Appendix which is comprised of tables in a form normally used by MSFC in summarizing fracture analysis results. In many instances the applied stress levels were so low that the threshold stress intensity factor range was never reached. In most of the others the allowable flaw sizes were large enough to be detected by visual inspection. However, for some parts, such as the flexures connecting the aluminum cover to the ball retainer in the fitting at point A, the flaw sizes were rather small. Eddy current tests are capable of detecting flaws of this size (0.022 inches x 0.1 inches), so for those which have been so tested these small flaws should represent no danger of going undetected.

In every instance approximations were made to err on the conservative side. These were pointed out in the discussions of the analyses for each fitting. One conservative approximation that was not mentioned, however, is the fact that retardation was not included in the crack propagation computations. It is probable that retardation occurs after Steps 8 and 16 in the load spectrum of Table 2, and so it is

expected that the predicted crack growth rates are larger than they are in reality resulting in smaller predicted allowable flaw sizes than actually may be tolerated.

TABLES

TABLE 1 RADIAL SI LOADS

Force	Acoustic (kips)	Lift-Off (kips)	Landing (kips)
A_1	0.771	2.372	1.660
A_2	0.298	0.770	0.425
A_3	0.660	2.014	1.894
B_1	1.213	3.459	2.091
C_1	1.208	3.440	2.082
C_2	0.958	2.148	0.987

TABLE 2 RADIAL SI LATCHES LOAD SPECTRUM

σ_A : Stresses Calculated Using Acoustic Loads

σ_{LO}: Stresses Calculated Using Lift-Off Loads

σ_L : Stresses Calculated Using Landing Loads

Event	Step	Maximum	Minimum	Cycles
Acoustics	1	$1/3 \times \sigma_A$	$1/3 \times \sigma_A$	1417
	2	$2/3 \times \sigma_A$	$2/3 \times \sigma_A$	1696
	3	σ_A	σ_A	487
Ship	4	$.39 \times \sigma_L$	$.20 \times \sigma_L$	155
	5	$.37 \times \sigma_L$	$.22 \times \sigma_L$	799
	6	$.35 \times \sigma_L$	$.24 \times \sigma_L$	13837
	7	$.33 \times \sigma_L$	$.25 \times \sigma_L$	218378
Launch	8	σ_{LO}	σ_{LO}	4
	9	$.75 \times \sigma_{LO}$	$.75 \times \sigma_{LO}$	7
	10	$.50 \times \sigma_{LO}$	$.50 \times \sigma_{LO}$	13
	11	$.25 \times \sigma_{LO}$	$.25 \times \sigma_{LO}$	30
Landing	12	σ_L	σ_L	4
	13	$.75 \times \sigma_L$	$.75 \times \sigma_L$	5
	14	$.50 \times \sigma_L$	$.50 \times \sigma_L$	10
	15	$.25 \times \sigma_L$	$.25 \times \sigma_L$	4
Launch	16	σ_{LO}	σ_{LO}	4
	17	$.75 \times \sigma_{LO}$	$.75 \times \sigma_{LO}$	7
	18	$.50 \times \sigma_{LO}$	$.50 \times \sigma_{LO}$	13
	19	$.25 \times \sigma_{LO}$	$.25 \times \sigma_{LO}$	30
Landing	20	σ_L	σ_L	4
	21	$.75 \times \sigma_L$	$.75 \times \sigma_L$	5
	22	$.50 \times \sigma_L$	$.50 \times \sigma_L$	10
	23	$.25 \times \sigma_L$	$.25 \times \sigma_L$	4

Table 3. Point A Fitting Fracture Susceptibility

Part Name	Part No.	Material	ΔK_o (ksi $\sqrt{inch}$)	K_c (ksi $\sqrt{inch}$)	Fracture Susceptibility
FPS:					
Base	679-3973	TI 6AL-4V	6	80	NCG
Flexure	679-4132	PH13-8 Mo	7	95	TEB, a_o = 0.022"
Cover	679-4135	7075-T73	3.5	40	NCG
Bolt	679-5280	PH13-8 Mo	7	95	C, a_o = 0.035" (NSY)
Lower Retainer	679-4130-111	TI 6AL-4V	6	80	C, a_o = 0.011"
Retainer Bolts	NAS 1351	Steel, S_{ut}=80 ksi	--	--	F-S
Base Bolts	NAS 1005	A 286	--	--	F-S
SI:					
Base	679-2152	TI 6AL-4V	6	80	NCG
Jackhead	679-2230	PH13-8 Mo	7	95	C, a_o = 0.032" (NSY)
Base Bolts	NAS 1005	A 286	--	--	F-S

Key: C = Circumferential Flaw, TEB = Through Edge Beam, F-S = Fail-Safe, NCG = No Crack Growth, NSY = Net Section NSY = Net Section Yielding

Table 4. Point B Fitting Fracture Susceptibility

Part Name	Part No.	Material	ΔK_o (ksi $\sqrt{inch}$)	K_c (ksi $\sqrt{inch}$)	Fracture Susceptibility
FPS:					
Base*	911-4338	TI 6AL-4V	6	80	NCG
Ball*	679-2387-110	PH13-8 Mo	7	95	C, a_o = 0.1475" (NSY)
Bolts*	NAS 1005	A 286	--	--	F-S
SI:					
Support Plate	679-2228	TI 6AL-4V	6	80	TEB, a_o = 0.153"
Base*	679-2211	TI 6AL-4V	6	80	NCG
Bolts* (SP/Base)	NAS 1005	A 286	15	100	C, a_o = 0.027" (NSY)
Bolts* (Base/SI)	NAS 1005	A 286	--	--	F-S

Key: * - Results obtained from Point C Fitting analyses

C - Circumferential Flaw, TEB = Through Edge Beam, F-S = Fail-Safe, NCG = No Crack Growth

NSY - Net Section Yielding

Table 5. Point C Fitting Fracture Susceptibility

Part Name	Part No.	Material	ΔK_o (ksi $\sqrt{inch}$)	K_c (ksi $\sqrt{inch}$)	Fracture Susceptibility
FPS:					
Base	911-4236	TI 6AL-4V	6	80	NCG
Ball	679-2387-110	PH13-8 Mo	7	95	C, a_o = 0.1475" (NSY)
Bolts	NAS 1005	A 286	--	--	F-S
SI:					
Support Plate	679-2223	TI 6AL-4V	6	80	TEB, a_o = 0.21" (NSY)
Base	679-2211	TI 6AL-4V	6	80	NCG
Bolts (SP/Base)	NAS 1005	A 286	15	100	C, a_o = 0.027"(NSY)
Bolts (Base/SI)	NAS 1005	A 286	--	--	F-S

Key: C = Circumferential Flaw, TEB = Through Edge Beam, F-S = Fail-Safe, NCG = No Crack Growth, NSY = Net Section Yielding

FIGURES

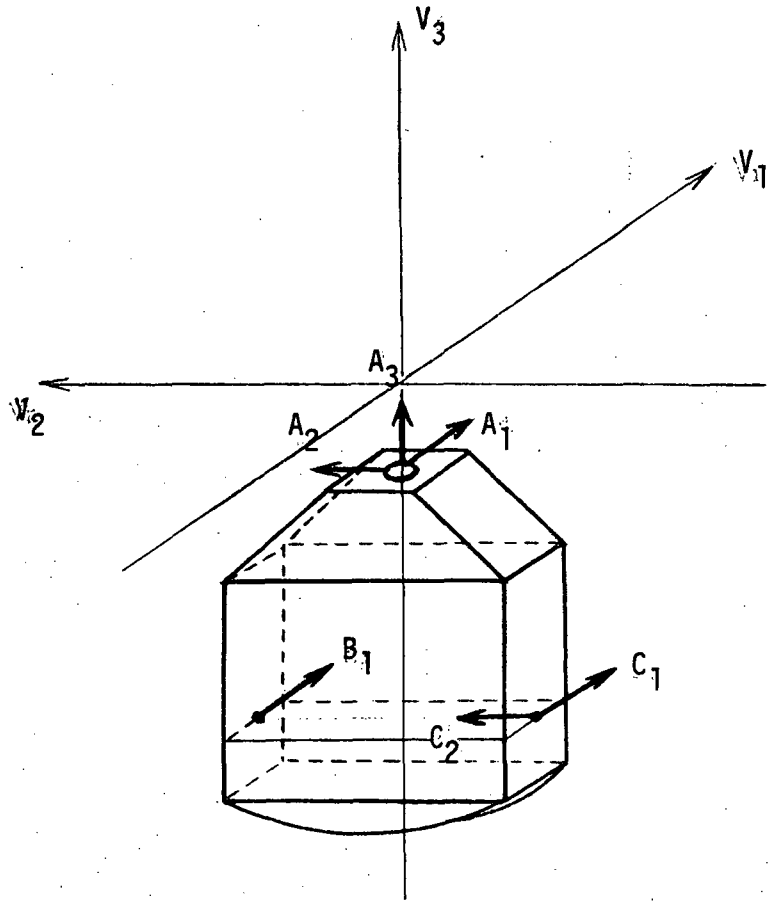

Figure 1. Radial SI in $-V_3$ Bay

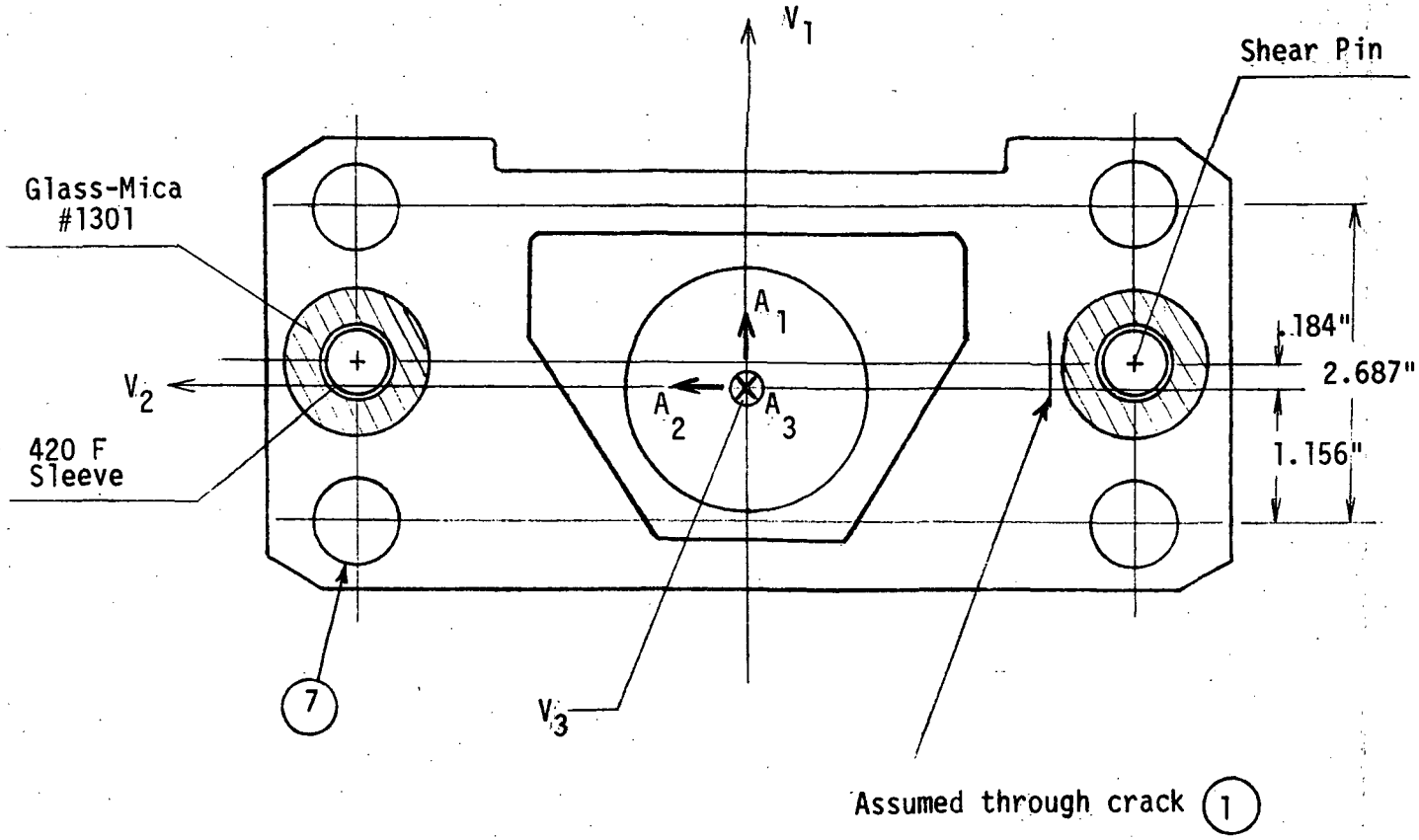

Figure 2. Base (679-3973)

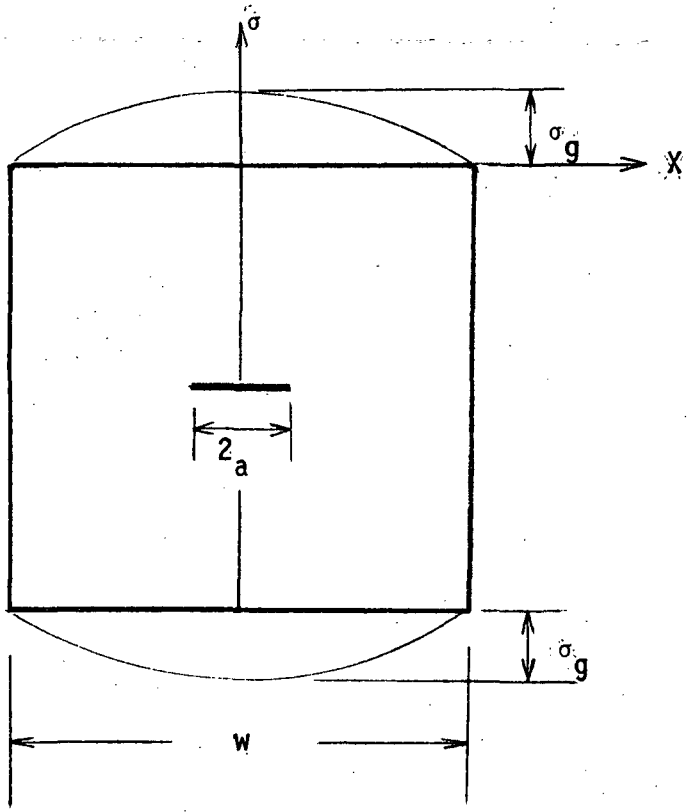

$$\sigma = \sigma_g \cos\left(\frac{\pi x}{W}\right)$$

Figure 3. Central Through Crack Model

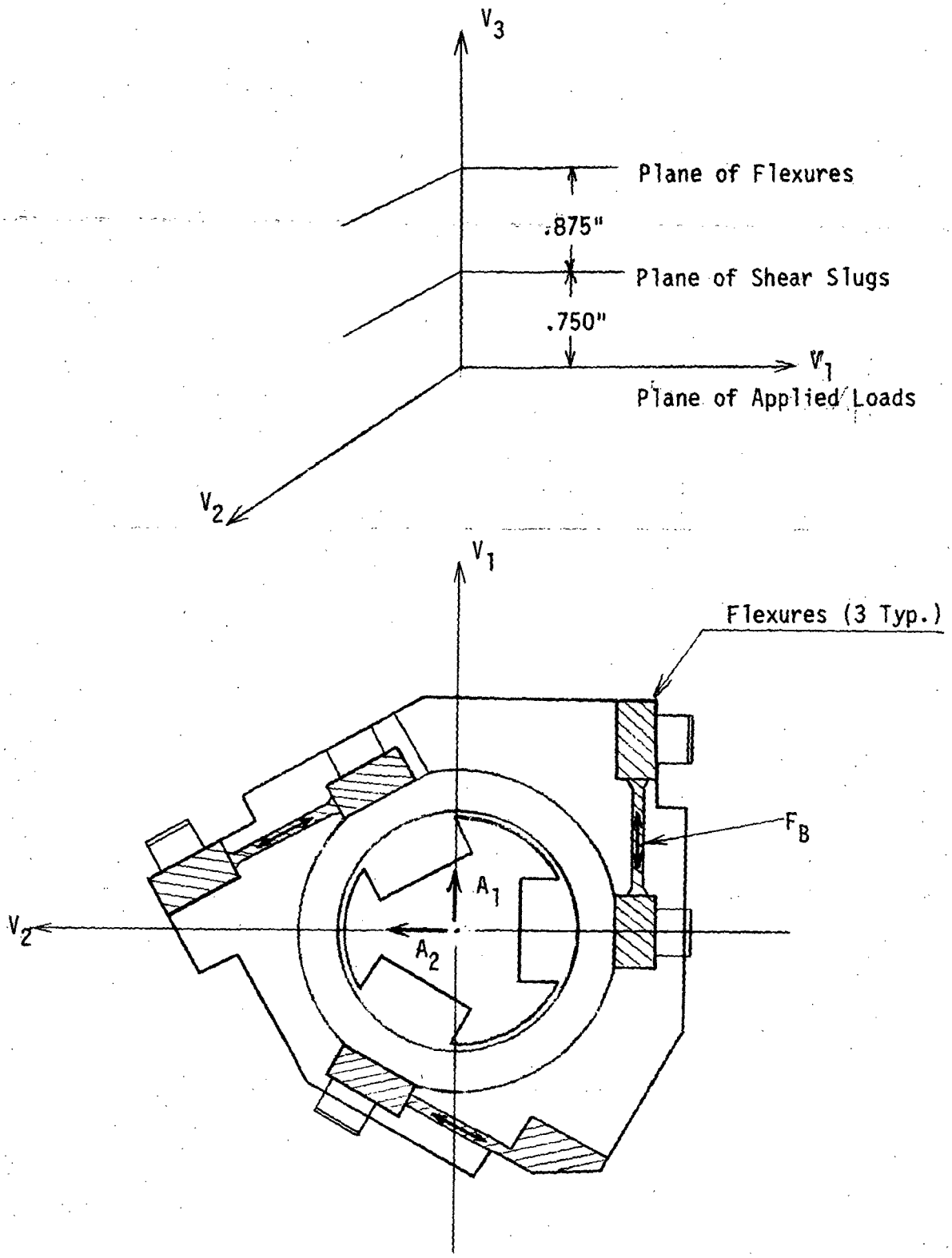

Figure 4. Locations of the Flexures and the Shear Slugs

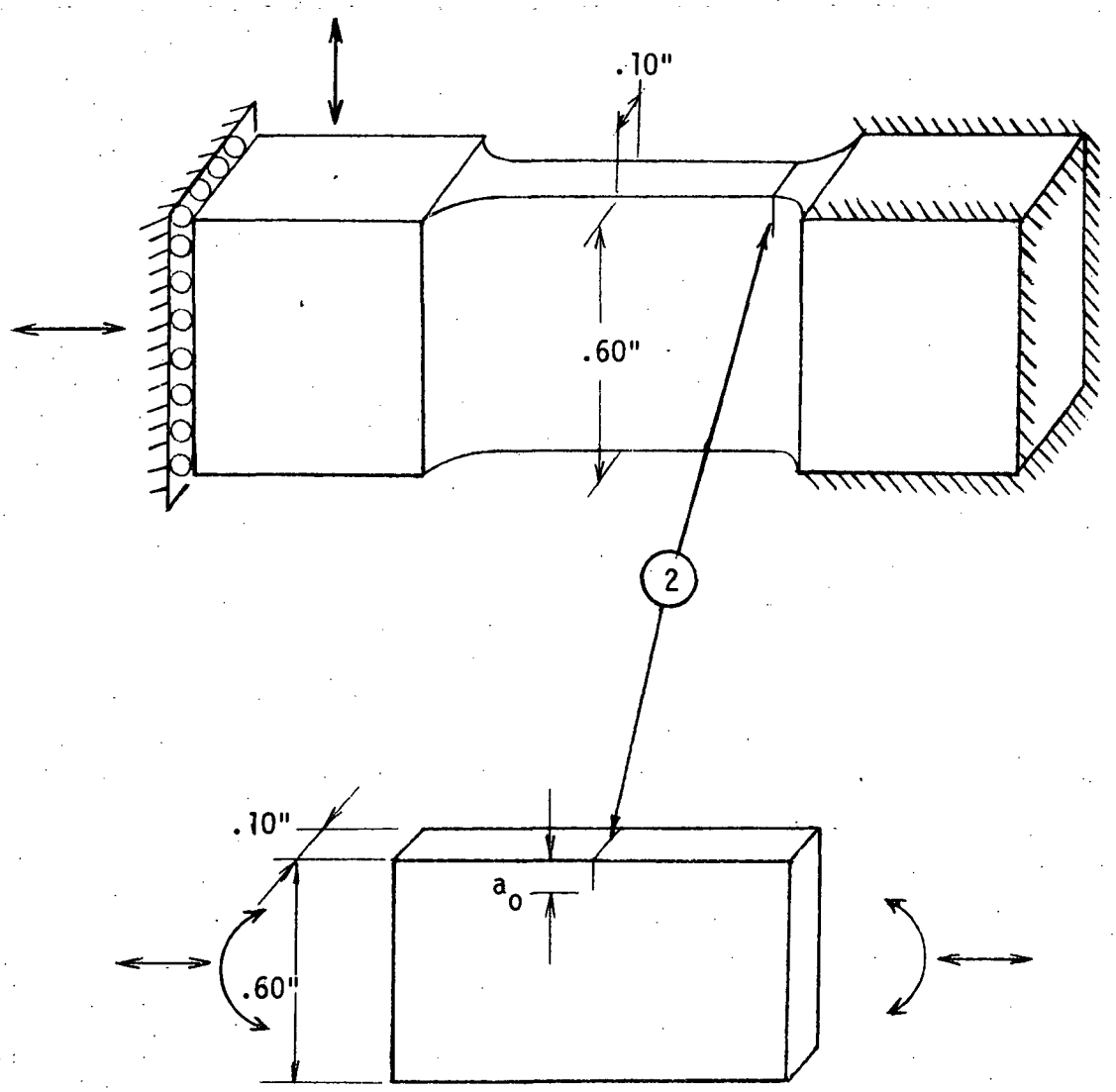

Figure 5. Flexure (679-4132) and Edge Crack Model

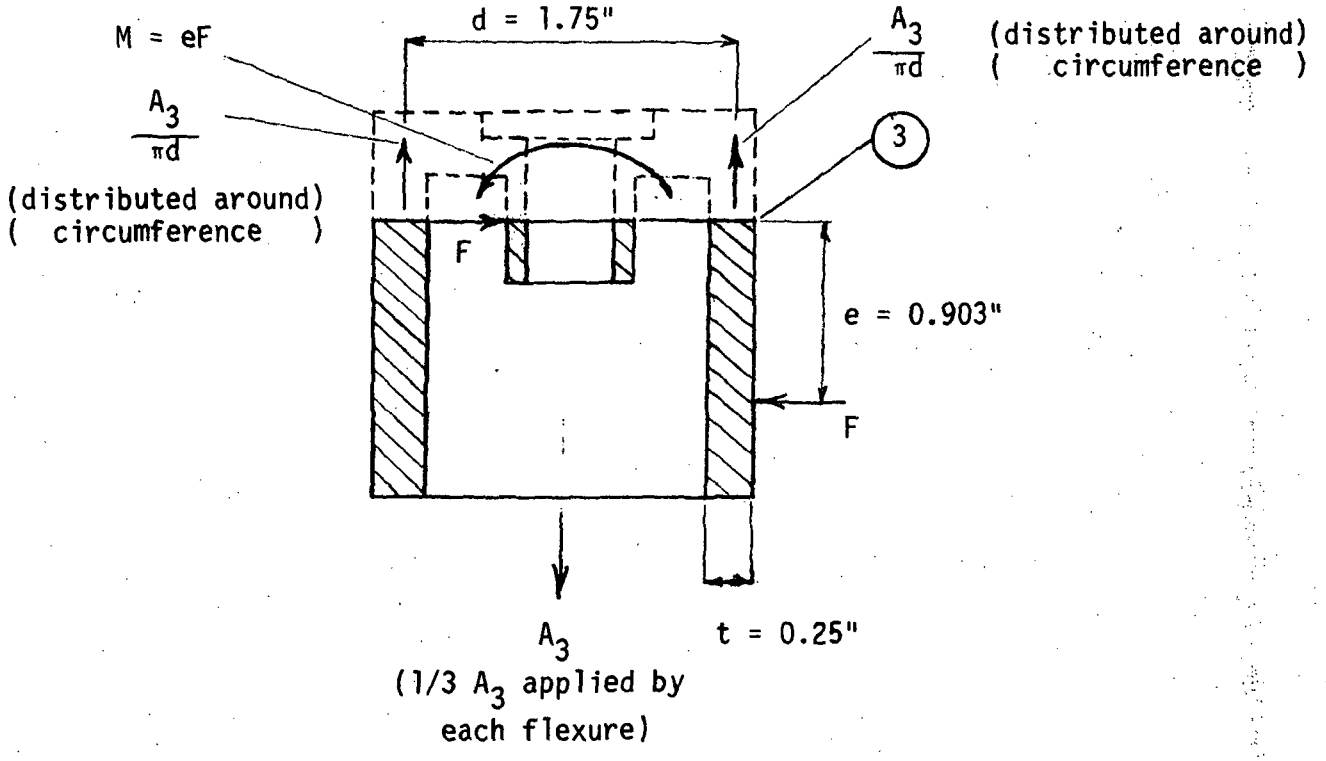

Figure 6. Section Through Aluminum Cover (679-4135) Showing Applied Loads and Reactions

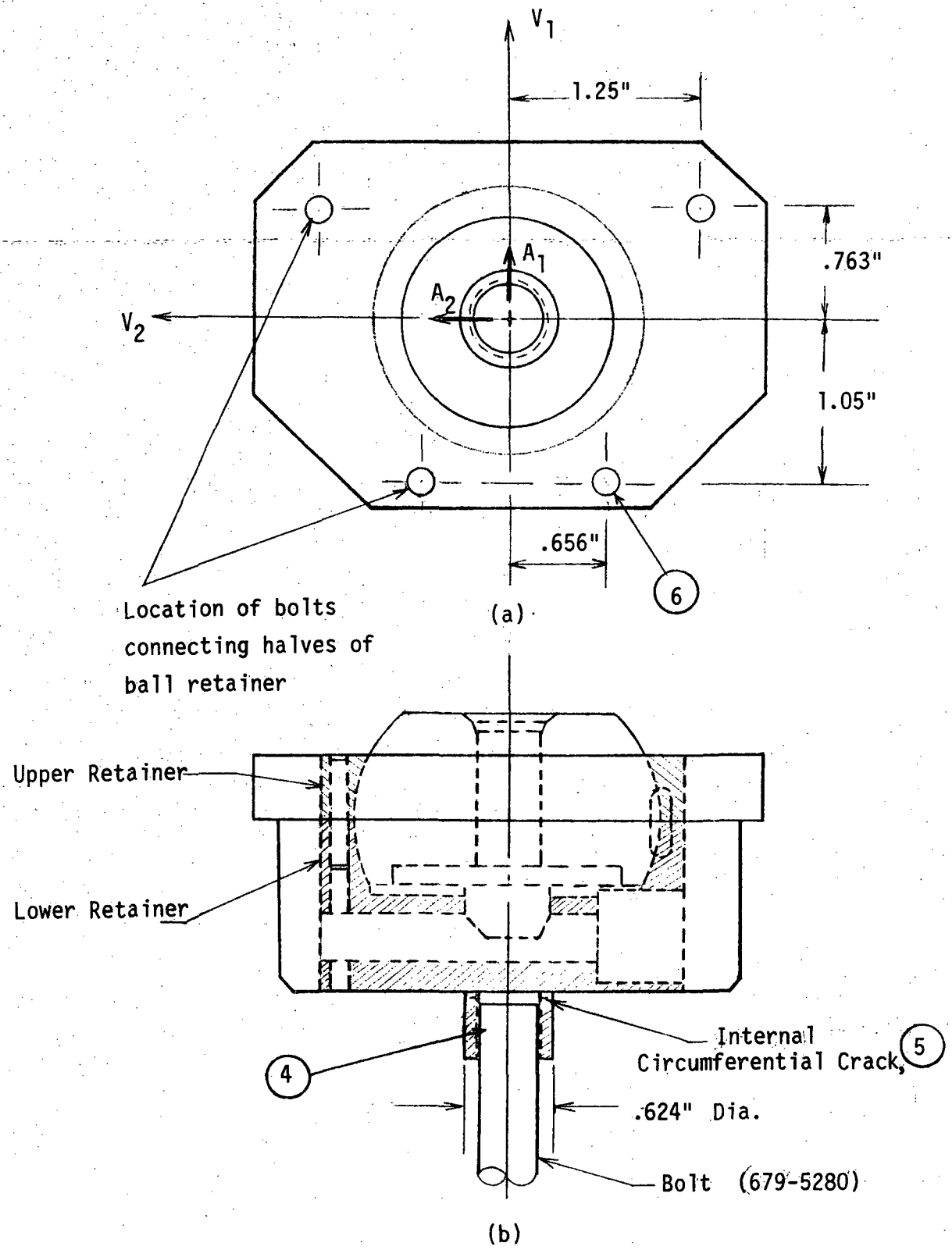

Figure 7. Ball Retainer (679-4130)

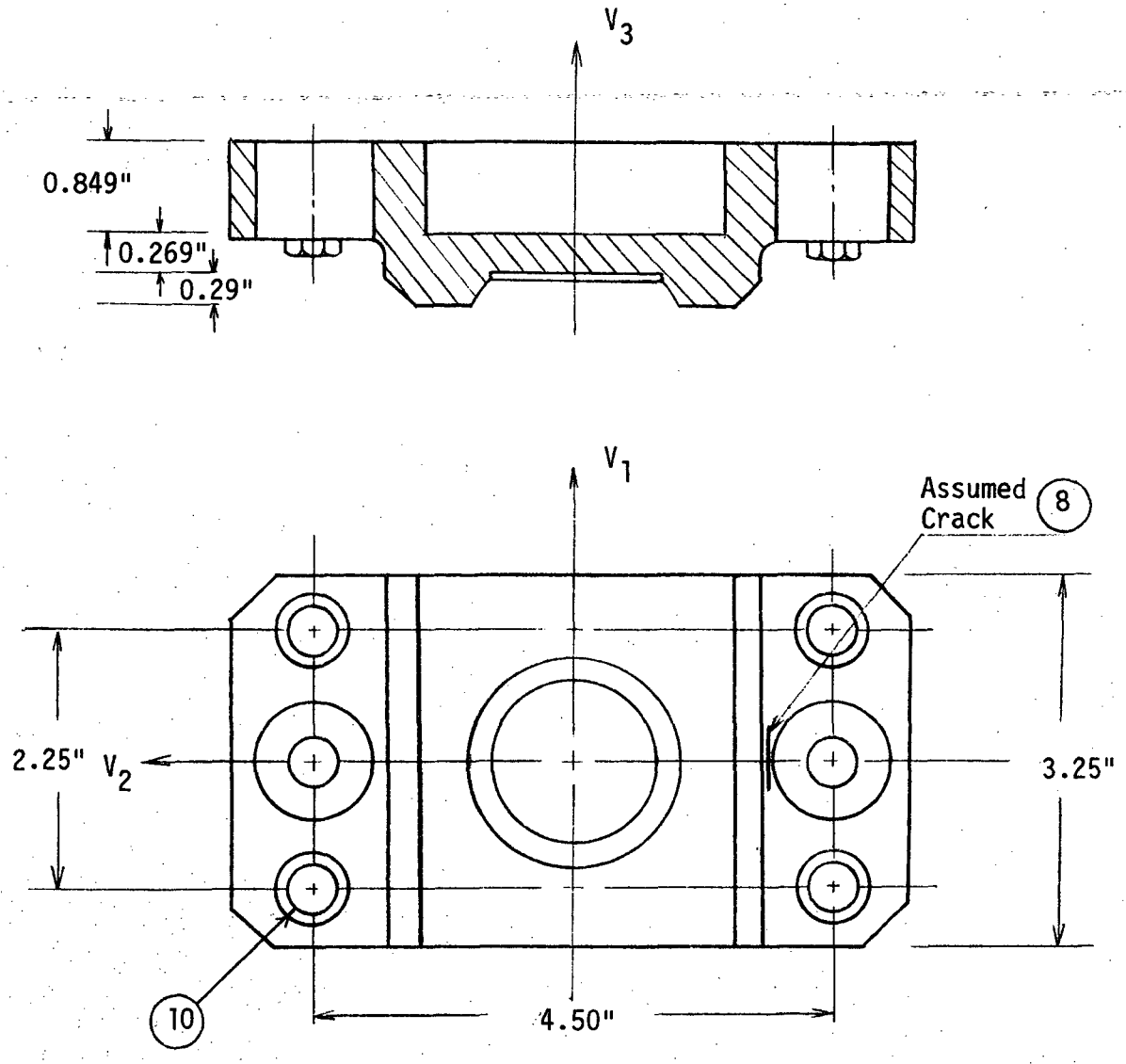

Figure 8. Point A Base, SI Side (679-2152)

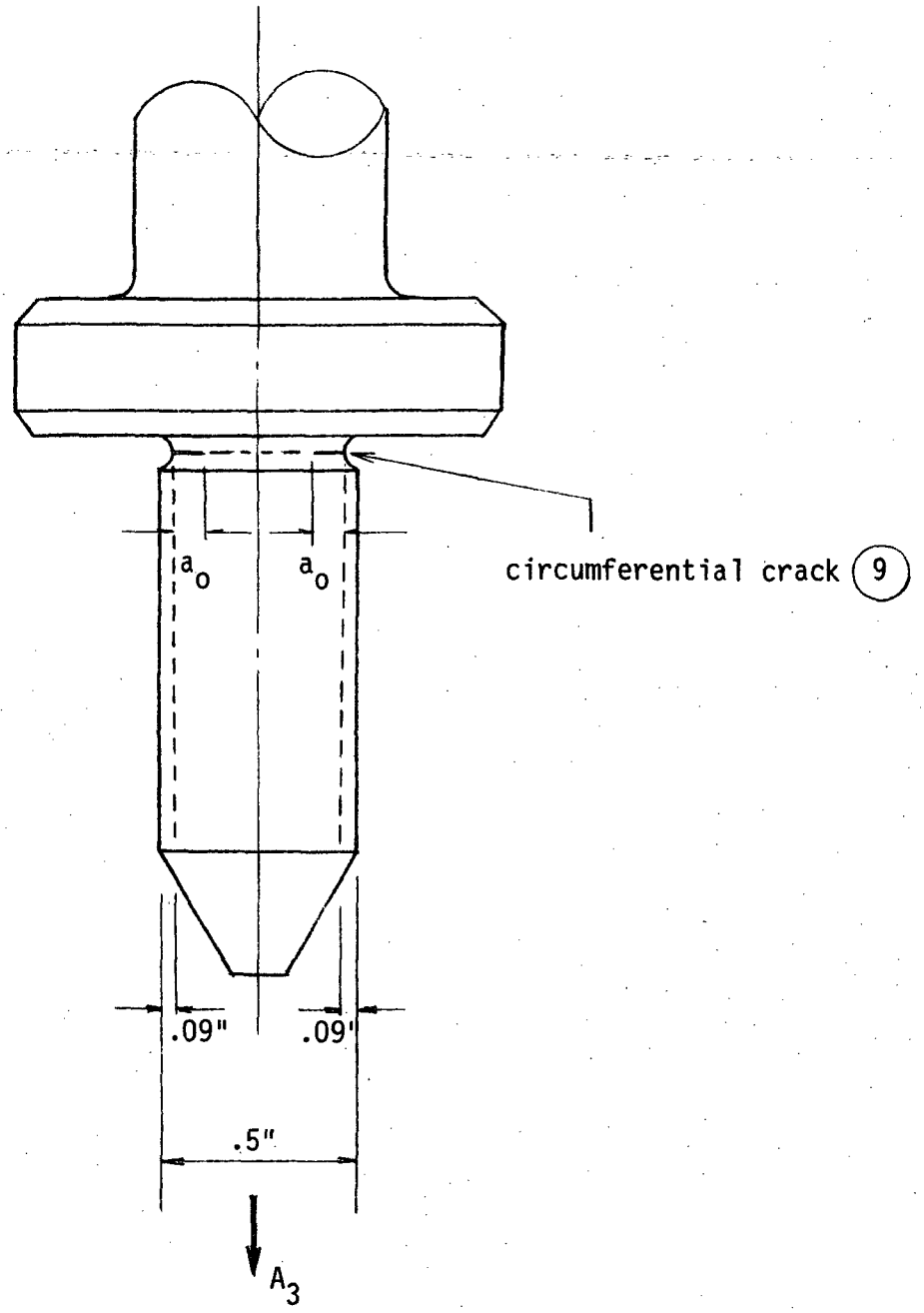

Figure 9. Jackhead

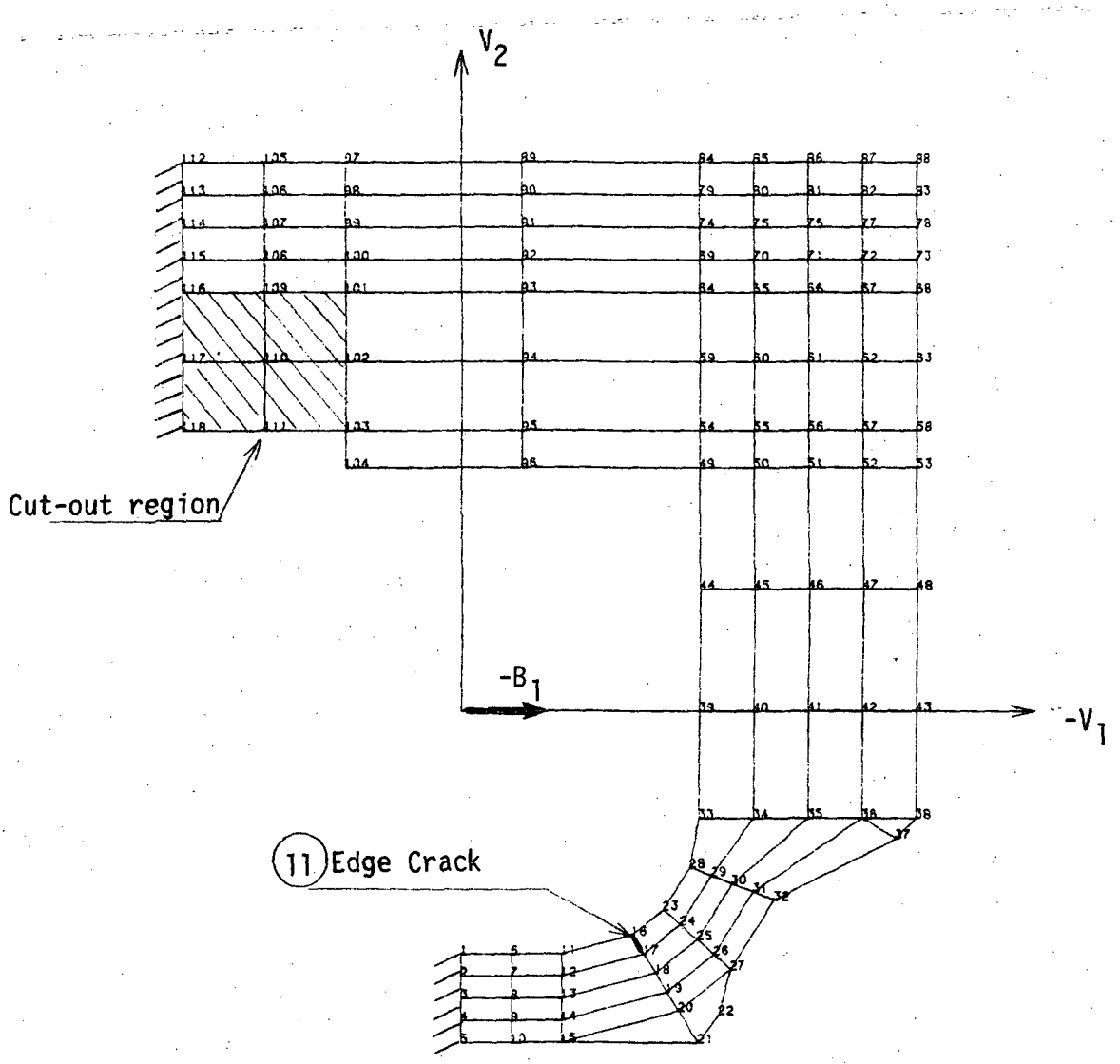

Figure 10. Finite Element Model of Point B Support Plate

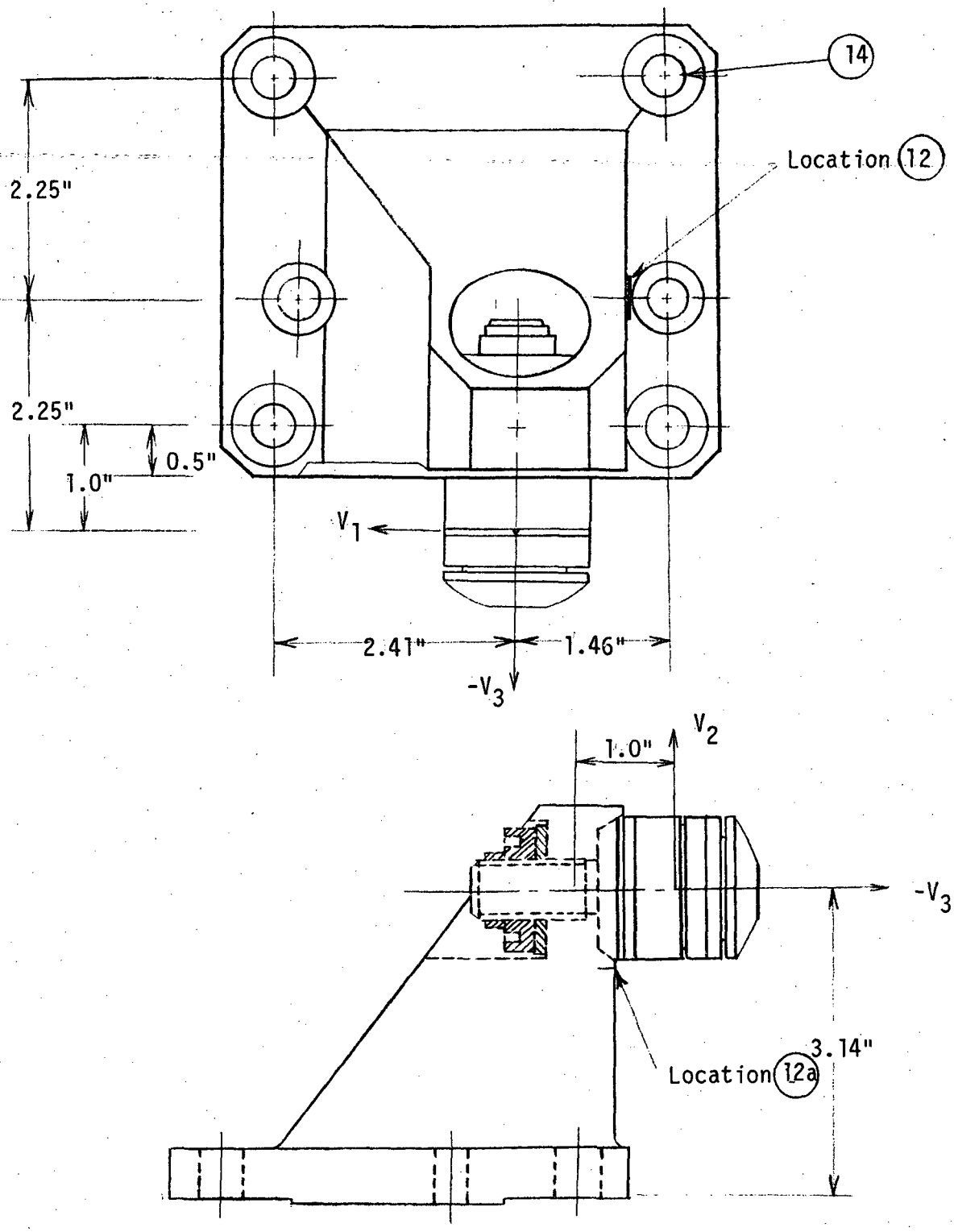

Figure 11. Point C Base, FPS Side (911-4236)

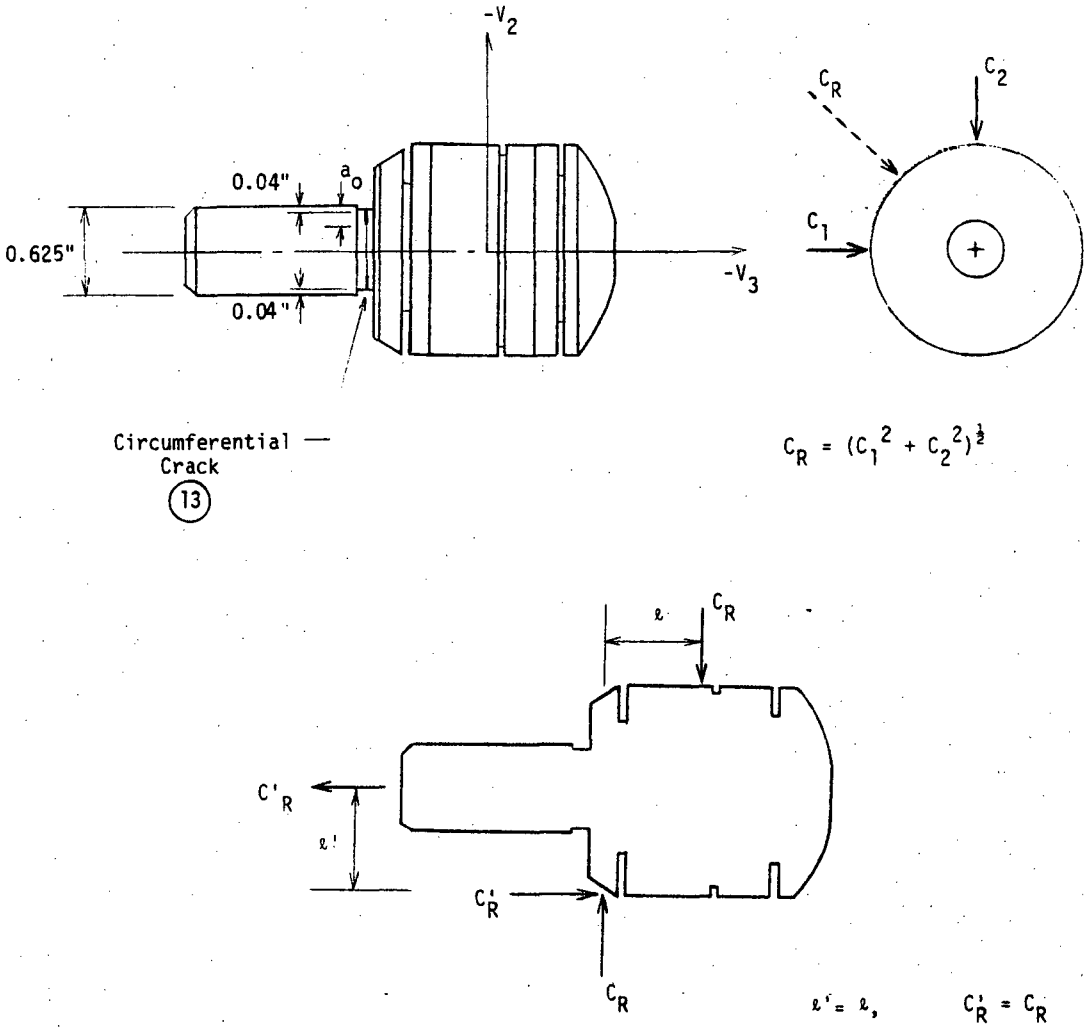

Figure 12. Circumferential Flaw of the Bolt

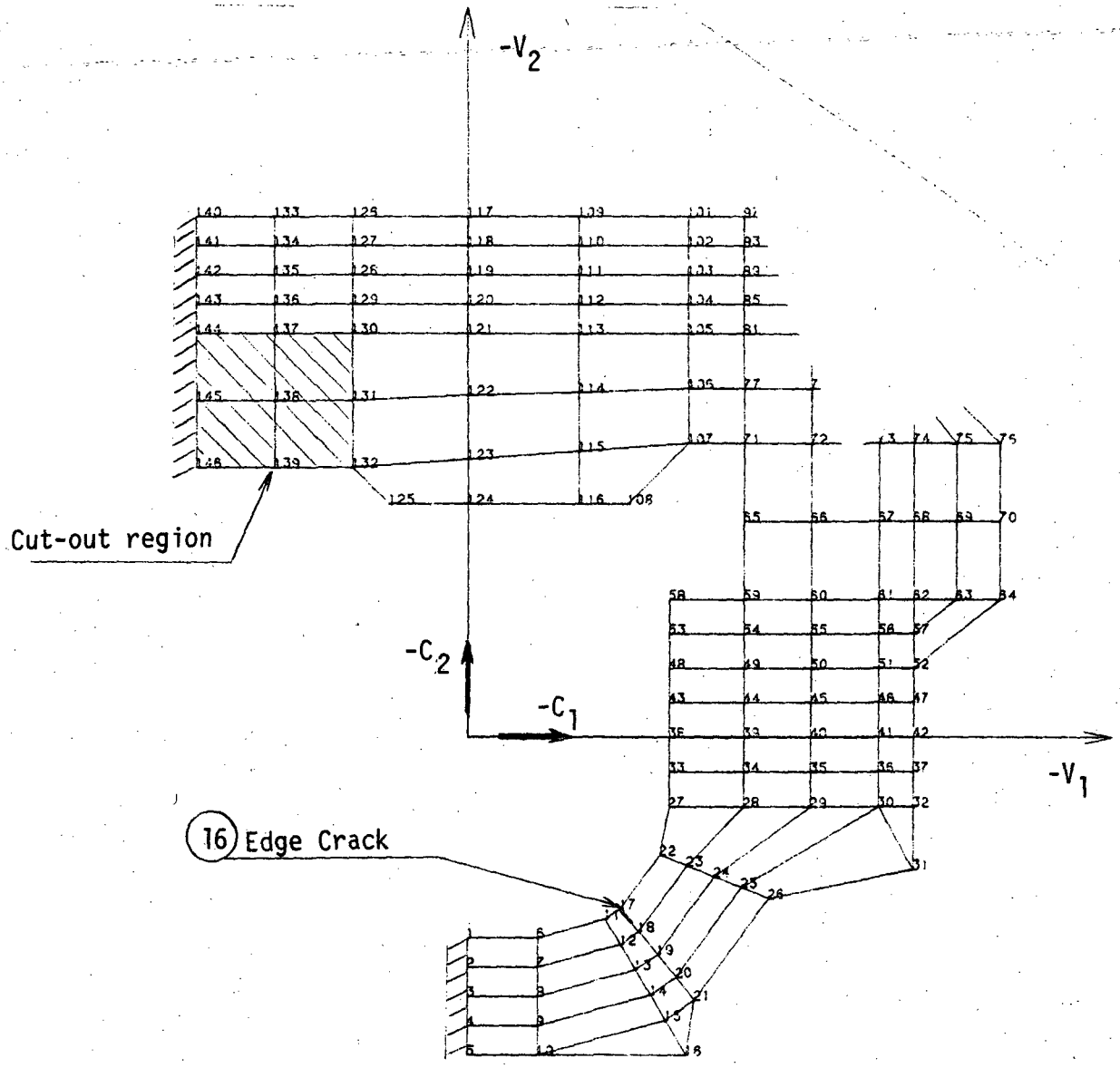

Figure 13. Finite Element Model of Point C Support Plate

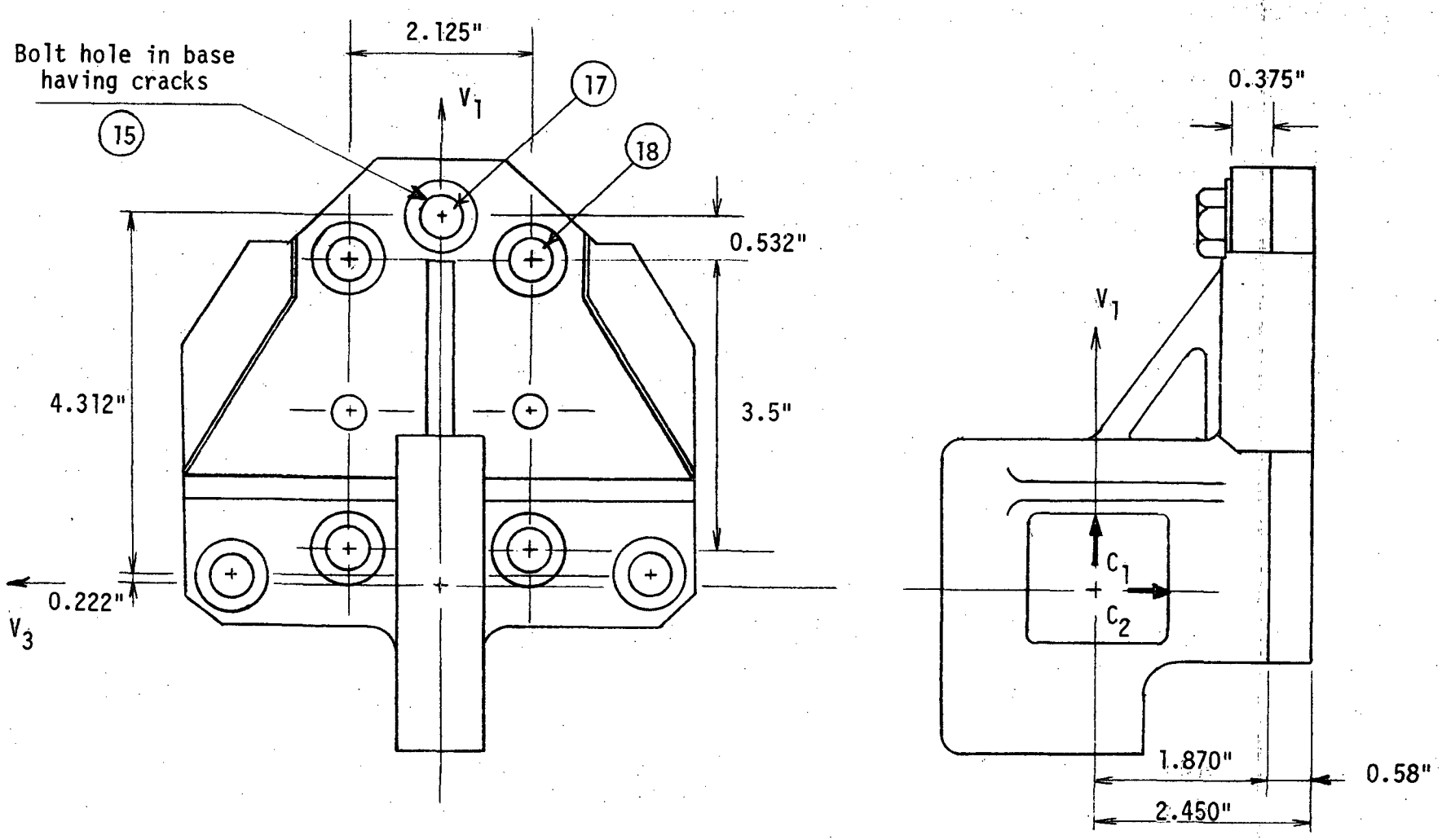

Figure 14. Point C Base (679-2211) and Support Plate (679-2223)

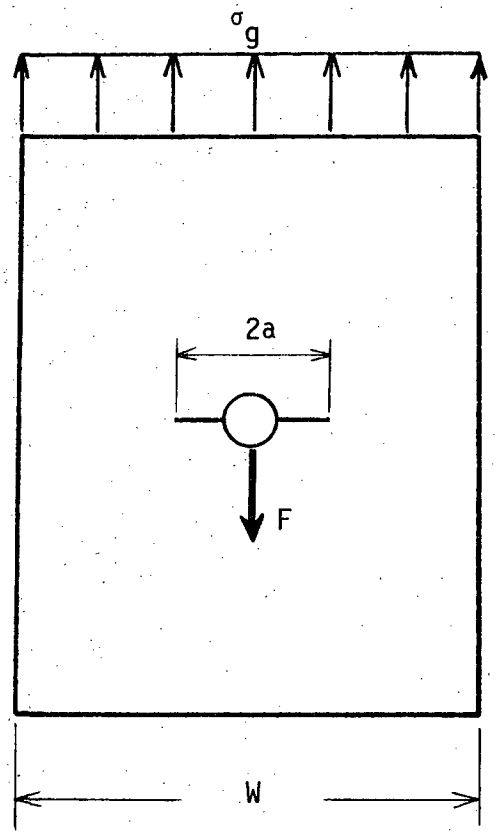

$$F = t \times W \times \sigma_g$$

$$K_I = \frac{\sigma_g}{2}\left[\sqrt{\pi a} + \frac{W}{\sqrt{\pi a}}\right]$$

Figure 15. Bolt Hole Crack Model

REFERENCES

1. Hu, T., Advanced Crack Propagation Predictive Analysis Computer Program "FLAGRO4", Rockwell International, September 1979.

2. Collipriest, J.E., Jr., "Experimentalists' View of the Surface Flaw Problem", Surface Crack: Physical Problems and Computational Solutions, ASME, NY, 1972, p. 43-61.

3. Anonymous, SAP V: A Structural Analysis Program for Static an Dynamic Response of Linear Systems - User's Manual, SAP Users Group, University of Southern California, October 1977.

APPENDIX

ORGANIZATION:	MARSHALL SPACE FLIGHT CENTER	NAME:
CHART NO.:	SPACE TELESCOPE FRACTURE CONTROL	DATE:

ASSEMBLY Space Telescope

SUBASSEMBLY Radial SI, Point A, FPS Half

PART NAME	PART NUMBER	PART SIZE (IN)*	MATERIAL	FLAW DEPTH (IN)	FLAW LENGTH (IN)	FLAW TYPE	LIFE-TIME	STRESS (KSI)	SF / KEY
Base	679-3973	t = 0.718 w = 3.0	TI-6AL-4V	0.718	>2.0	TC	4	0.3	>10 / 1
Flexure	679-4132	t = 0.6 w = 0.1	PH13- 8 Mo	0.022	0.1	TEB	4	61	3.3 / 2
Cover	679-4135	t = 0.25 w = 2.75	7075-T73	0.25	>1.3	TC	4	5.1	>10 / 3
Bolt	679-5280	d = 0.4375	PH13 - 8 Mo	0.035	1.374	C	4	85	2.36 / 4
Lower Retainer	679-4130-111	t = 0.126 w = 1.61	TI-6AL-4V	0.011	1.61	TEB	4	63	2.06 / 5
Retainer Bolts	NAS 1351	d = .3125	Steel, S_{ut}=80	--	--	F-S	-	76	1.05 / 6
Base Bolts	NAS 1005	d = .4375	A 286	--	--	F-S	-	102	1.37 / 7

NOTES: *Size used in fracture mechanics model, t x w, diameter, etc.

TC - Through Center
TEB - Through Edge Beam
C - Circumferential Flaw
F-S - Fail-Safe Analysis

ORGANIZATION:	MARSHALL SPACE FLIGHT CENTER	NAME:
CHART NO.:	SPACE TELESCOPE FRACTURE CONTROL	DATE:

ASSEMBLY Space Telescope

SUBASSEMBLY Radial SI, Point A, SI Half

PART NAME	PART NUMBER	PART SIZE (IN)*	MATERIAL	FLAW			LIFE-TIME	STRESS (KSI)	SF / KEY
				DEPTH (IN)	LENGTH (IN)	TYPE			
Base	679-2152	t = 0.88 w = 3.24	TI 6AL-4V	0.88	> 2.0	TC	4	0.2	>10 / 8
Jackhead	679-2230	d = 0.5	PH13 - 8 Mo	0.032	1.57	C	4	45.3	4.44 / 9
Base Bolts	NAS 1005	d = .4375	A 286	--	--	F-S	-	116	1.21 / 1.0

NOTES: *Size used in fracture mechanics model, t x w, diameter, etc.

TC - Through Center Crack
C - Circumferential Flaw
F-S - Fail-Safe Analysis

ORGANIZATION:	MARSHALL SPACE FLIGHT CENTER	NAME:
CHART NO.:	SPACE TELESCOPE FRACTURE CONTROL	DATE:

ASSEMBLY Space Telescope

SUBASSEMBLY Radial SI, Point B, FPS Half

PART NAME	PART NUMBER	PART SIZE (IN)*	MATERIAL	FLAW			LIFE-TIME	STRESS (KSI)	SF / KEY
				DEPTH (IN)	LENGTH (IN)	TYPE			
Base+	911-4338	t = 0.5 w = 4.5	TI 6AL-4V	0.5	2.0	TC	4	1.2	>10 / 12
Ball+	679-2387-110	d = 0.625	PH13 - 8 Mo.	.1475	1.96	C	4	27.6	7.28 / 13
Bolts+	NAS 1005	d = 0.4375	A 286	--	--	F-S	-	101	1.39 / 14

NOTES: *Size used in fracture mechanics model, t x w, diameter, etc.

TC - Through Center Crack
C - Circumferential Flaw
F-S - Fail-Safe Analysis

+These results obtained from analyses of point C fitting.

ORGANIZATION:	MARSHALL SPACE FLIGHT CENTER	NAME:
CHART NO.:	SPACE TELESCOPE FRACTURE CONTROL	DATE:

ASSEMBLY Space Telescope

SUBASSEMBLY Radial SI, Point B, SI Half

PART NAME	PART NUMBER	PART SIZE (IN)*	MATERIAL	FLAW			LIFE-TIME	STRESS (KSI)	SF / KEY
				DEPTH (IN)	LENGTH (IN)	TYPE			
Base+	679-2211	t = 0.58 w = 2.125	TI 6AL-4V	0.58	>2.0	TC	4	0.9	>10 / 15
Support Plate	679-2228	t = 0.31 w = 1.0	TI 6AL-4V	0.153	1.0	TEB	4	18.7	6.95 / 11
Bolts (SP/Base)+	NAS 1005	d = 0.4375	A 286	0.027	1.37	C	4	30.4	4.61 / 17
Bolts (Base/SI)+	NAS 1005	d = 0.4375	A 286	--	--	F-S	-	89.5	1.56 / 18

NOTES: *Size used in fracture mechanics model, t x w, diameter, etc.

TC - Through Center Crack
TEB - Through Edge Beam
C - Circumferential Flaw
F-S - Fail-Safe Analysis
+These results obtained from analyses of point C fitting.

ORGANIZATION:	MARSHALL SPACE FLIGHT CENTER	NAME:
CHART NO.:	SPACE TELESCOPE FRACTURE CONTROL	DATE:

ASSEMBLY Space Telescope

SUBASSEMBLY Radial SI, Point C, FPS Half

PART NAME	PART NUMBER	PART SIZE (IN)*	MATERIAL	FLAW			LIFE-TIME	STRESS (KSI)	SF / KEY
				DEPTH (IN)	LENGTH (IN)	TYPE			
Base	911-4236	t = 0.5 w = 4.5	TI 6AL-4V	0.5	>2.0	TC	4	1.2	>10 / 12
Ball	679-2387-110	d = 0.625	PH13 - 8 Mo.	.1475	1.96	C	4	27.6	7.28 / 13
Bolts	NAS 1005	d = 0.4375	A286	--	--	F-S	-	101	1.39 / 14

NOTES: *Size used in fracture mechanics model, t x w, diameter, etc.

TC - Through Center Crack
C - Circumferential Flaw
F-S - Fail-Safe Analysis

ORGANIZATION:	MARSHALL SPACE FLIGHT CENTER	NAME:
CHART NO.:	**SPACE TELESCOPE FRACTURE CONTROL**	DATE:

ASSEMBLY Space Telescope

SUBASSEMBLY Radial SI, Point C, SI Half

PART NAME	PART NUMBER	PART SIZE (IN)*	MATERIAL	FLAW			LIFE-TIME	STRESS (KSI)	SF / KEY
				DEPTH (IN)	LENGTH (IN)	TYPE			
Base	679-2211	t = 0.58 w = 2.125	TI 6AL-4V	0.58	>2.0	TC	4	0.9	>10 / 15
Support Plate	679-2223	t = 0.42 w = 1.0	TI 6AL-4V	0.21	1.0	TEB	4	18.7	6.95 / 16
Bolts (SP/Base)	NAS 1005	d = .4375	A 286	0.027	1.37	C	4	30.4	4.61 / 17
Bolts (Base/SI)	NAS 1005	d = .4375	A 286	--	--	F-S	-	89.5	1.56 / 18

NOTES: *Size used in fracture mechanics model, t x w, diameter, etc.

TC - Through Center
TEB- Through Edge Beam
C - Circumferential Flaw
F-S - Fail-Safe Analysis